Food Safety and Health

WILEY

RESEARCH ARTICLE OPEN ACCESS

Exploring the Multifunctional Agents of Flavonoid-Rich Beet Leaf Extracts: Insights From Experimental and Computational Studies

Gideon Ampoma Gyebi[1,2] | Damilare Emmanuel Rotimi[3,4] | Moyosoreoluwa Oduba[5] | Ifeoma Nnonyelu[5] | Matthew Iyobhebhe[3] | Musiliyu Ayofe Salawu[6] | Adebola Busola Ojo[7] | Odunayo Anthonia Taiwo[8] | Adesoji Alani Olanrewaju[9] | Abel Kolawole Oyebamiji[10] | Mubarak Alruwaili[11] | Naif H. Ali[12] | Saud A. Alnaaim[13] | Bshra A. Alsfouk[14] | Gaber El-Saber Batiha[15] | Oluwafemi Adeleke Ojo[16]

[1]Durban University of Technology, Durban, South Africa | [2]Department of Biotechnology and Food Science, Faculty of Applied Sciences, Durban University of Technology, Durban, South Africa | [3]Department of Biochemistry, Landmark University, Omu-Aran, Nigeria | [4]Department of Pharmacology and Pharmaceutical Sciences, Alfred E. Mann School of Pharmacy and Pharmaceutical Sciences, University of Southern California, Los Angeles, California, USA | [5]Department of Biochemistry, Phytomedicine, Molecular Toxicology, and Computational Biochemistry Research Group, Bowen University, Iwo, Nigeria | [6]Department of Biochemistry, Fountain University, Osogbo, Nigeria | [7]Department of Environmental Management and Toxicology, University of Ilesa, Ilesa, Nigeria | [8]Department of Biochemistry, Chrisland University, Abeokuta, Nigeria | [9]Department of Chemistry and Industrial Chemistry, Bowen University, Iwo, Nigeria | [10]Department of Industrial Chemistry, University of Ilesa, Ilesa, Nigeria | [11]Department of Internal Medicine, College of Medicine, Jouf University, Sakaka, Saudi Arabia | [12]Department of Internal Medicine, Medical College, Najran University, Najran, Saudi Arabia | [13]Clinical Neurosciences Department, College of Medicine, King Faisal University, Hofuf, Saudi Arabia | [14]Department of Pharmaceutical Sciences, College of Pharmacy, Princess Nourah bint Abdulrahman University, Riyadh, Saudi Arabia | [15]Department of Pharmacology and Therapeutics, Faculty of Veterinary Medicine, Damanhour University, Damanhour, Egypt | [16]Research Centre for Integrative Physiology and Pharmacology, Institute of Biomedicine, University of Turku, Turku, Finland

Correspondence: Oluwafemi Adeleke Ojo (oluwafemiadeleke08@gmail.com)

Received: 6 May 2025 | **Revised:** 11 July 2025 | **Accepted:** 27 July 2025

Funding: The authors received no specific funding for this work.

Keywords: biocomputation | drug discovery | medicinal plants | noncommunicable diseases | pharmacology

ABSTRACT

This study evaluated the multifunctional ability of *Beta vulgaris* leaves in dual therapy for Alzheimer's disease (AD) and type 2 diabetes (T2D). Flavonoid-rich extracts of *B. vulgaris* leaves (FREBVL) were tested for their antidiabetic properties. The inhibition of α-amylase and α-glucosidase was assessed. Anti-cholinesterase activities against AChE, BchE, and monoamine oxidase were investigated. Molecular docking and dynamic simulations identified potential bioactive flavonoids. Compared with acarbose, FREBVL had moderate activity against α-amylase (IC_{50} = 102.808 ± 3.153 μg/mL) (IC50 = 27.104 ± 0.270 μg/mL). Appreciable activity against α-glucosidase (IC_{50} = 79.131 ± 1.129 μg/mL) was observed. The significant inhibitory activity against AChE (IC_{50} = 902.738 ± 1.199 μg/mL) was weaker than that of galantamine (IC_{50} = 27.950 ± 0.122 μg/mL). The notable inhibitory effects on BChE (IC_{50} = 143.742 ± 0.785 μg/mL) were comparable to those of galantamine (IC_{50} = 23.126 ± 0.683 μg/mL). FREBVL protected against Fe^{2+}-mediated brain damage by suppressing monoamine oxidase activity. Bioactive flavonoids (e.g., rutin, myricetin, apigenin) showed promising binding tendencies. Molecular dynamic simulations confirmed the stability of the complexes. FREBVL has potential as a multifunctional agent for dual therapy in T2D and AD.

1 | Introduction

On the basis of the data from Global Health and Aging (2010), the proportion of people over 65 years of age is expected to increase to 16%, with almost 426 million by 2050 (Padeiro et al. 2023). This demographic change underscores the pressing concern of age-related conditions, notably type 2 diabetes mellitus (T2DM) and Alzheimer's disease (AD). Without effective intervention, the convergence of these ailments poses a significant socioeconomic challenge in the future (Hernández-Contreras et al. 2023).

Alzheimer's disease (AD) is a chronic and irreversible neurodegenerative disease characterized by progressive memory loss and cognitive decline (O. A. Ojo et al. 2021). With an estimated 46.8 million people affected worldwide, this figure is projected to double by 2030 due to the absence of effective therapeutic interventions (Abeysinghe et al. 2020). Although we do not know exactly what causes AD, researchers have identified several factors that may play a role in its development, including reduced acetylcholine (ACh) levels, oxidative stress, and amyloid-β (Aβ) accumulation. Biometal dyshomeostasis was also observed. These factors are being studied as potential mechanisms underlying AD progression (Abeysinghe et al. 2020; Chen et al. 2022). The "cholinergic hypothesis" suggests that acetylcholinesterase (AChE) and butyrylcholinesterase (BuChE) play important roles in controlling cholinergic neurotransmission. By inhibiting both AChE and BuChE, we can potentially improve the management of Alzheimer's disease (AD). This approach increases the availability of acetylcholine (ACh) in the brain, which helps address cholinergic dysfunction (Moreira et al. 2022).

Type 2 diabetes mellitus (T2DM) is a common metabolic disorder that typically occurs as people age. It affects approximately 10% of the global population, with India, China, and the United States being identified as high-risk areas by the World Health Organization (Tinajero and Malik 2021). T2DM is characterized by cells becoming resistant to insulin, chronic inflammation, and various metabolic abnormalities (Reed et al. 2021). These factors lead to elevated blood sugar levels (hyperglycemia) and can cause complications in multiple organs, such as the liver, heart, kidneys, eyes (retina), and brain. One potential strategy to manage postmeal hyperglycemia involves inhibiting enzymes that breakdown carbohydrates, specifically α– and α–glucosidases, which delay glucose digestion (Tinajero and Malik 2021).

In recent years, increasing evidence from studies on populations, disease mechanisms, and genetics has suggested a connection between T2DM and Alzheimer's disease (AD) (Sun et al. 2020; Hardy et al. 2022; Lynn et al. 2022). Both conditions often occur together due to complex interactions that either promote or hinder the development of their respective pathological processes. Various factors contribute to their coexistence, including abnormal protein clumping, impaired insulin signaling, inflammation, oxidative stress, problems with energy production in cell powerhouses (mitochondria), excessive formation of harmful molecules called advanced glycation end products (ages), obesity, changes in gene activity without alterations to the DNA sequence (epigenetic modifications), impaired recycling of cellular components (autophagy), signaling problems involving a protein called transforming growth factor β (TGF-β), and genetic predispositions (Athanasaki et al. 2022; Hardy et al. 2022). However, we still do not fully understand the exact disease mechanisms that link T2DM and AD. A common early characteristic under both conditions is oxidative stress, which refers to an imbalance between harmful molecules called free radicals and the natural defense mechanisms that neutralize them. This imbalance becomes more pronounced as we age. As a result, there is interest in exploring the potential benefits of antioxidants, substances that can counteract free radicals, as treatments for AD and T2DM (Lynn et al. 2022).

Conventional medications for the treatment of AD and T2DM symptoms often have severe side effects and can lead to drug resistance with prolonged use. Therefore, the World Health Organization is focusing on developing safer herbal medicines. The use of this medicinal system since 2000 BC has led to the identification of plants with antidiabetic and neuroprotective properties (Wang et al. 2021; Richter et al. 2023). These plants have been used worldwide for treating AD and T2DM, but their effectiveness has not been scientifically proven.

One such plant is *Beta vulgaris*, commonly known as beet. It has various effects on the body, such as protecting the liver and kidneys, reducing inflammation, lowering blood sugar levels, and fighting harmful microorganisms (O. A. Ojo, Agboola, et al. 2023). *B. vulgaris* leaves, commonly known as beet greens, have been studied for their nutritional and phytochemical properties in animal feed. Research indicates that these leaves are rich in proteins, carbohydrates, fatty acids, vitamins, and fibers, making them a valuable source of nutrients for livestock (Iwuozor and Afiomah 2020). Studies have shown that incorporating *B. vulgaris* leaves into animal diets can improve growth performance, enhance the immune response, and provide antioxidant benefits because of their high contents of phenolic acids, flavonoids, and betalains. These findings suggest that *B. vulgaris* leaves could be a sustainable and health-promoting feed option for animals (Iwuozor and Afiomah 2020). However, there is very little research on whether beet leaves can be used as a dual treatment for AD and T2DM. Therefore, a systematic evaluation of flavonoid-rich extracts of *B. vulgaris* leaves is warranted to explore their anticholinesterase, antidiabetic, antioxidant, and neuroprotective activities, as well as their phytochemical profiles, to develop potent agents for dual therapy of AD and T2DM via experimental and computational studies.

2 | Materials and Methods

2.1 | Beet Leaf Collection

Leaves of *B. vulgaris* L. were sourced from the Jos Terminal Market, Plateau State, Nigeria. Plant identification was confirmed by the Forestry Research Institute of Nigeria (FHI 114105). The name was authenticated from the plantlist.org.

2.2 | Flavonoid-Rich Extract Preparation

Fifty grams (50 g) of powdered *B. vulgaris* leaves were subjected to maceration for 72 h using 80% methanol as the solvent, resulting in the extraction of a crude methanolic extract. We followed the method of O. A. Ojo et al. (2024) in the extraction of flavonoid-rich extracts from crude methanolic extracts.

2.3 | Determination of the Enzyme Inhibitory Activities of Flavonoid-Rich Extracts of *B. vulgaris* Leaves

2.3.1 | Alpha-Amylase Inhibitory Activity

The α-amylase inhibitory activity of flavonoid-rich extracts from *B. vulgaris* leaves was assessed via the method described by Shai et al. (2010). Acarbose served as the reference compound, and the experiment was conducted in triplicate. The percentage inhibition was calculated as follows:

$$\text{Percentage inhibition} = \frac{\text{Absorbance of control} - \text{Absorbance of sample}}{\text{Absorbance of control}} \text{x } 100$$

2.3.2 | Alpha-Glucosidase Inhibitory Activity

α-Glucosidase activity was measured spectrophotometrically at 400 nm using p-nitrophenyl-α-D-glucopyranoside (p-NPG) as the substrate, following the protocol of Loukili et al. (2022). Acarbose served as a positive control. The percent inhibition was calculated as follows:

$$\text{Percentage inhibition} = \frac{\text{Absorbance of control} - \text{Absorbance of sample}}{\text{Absorbance of control}} \text{x } 100$$

2.3.3 | Cholinesterase Activity

The enzyme inhibitory effects of *B. vulgaris* leaf extract on acetylcholinesterase (AChE) and butyrylcholinesterase (BChE) activities were determined following the protocol of Perry et al. (2000).

2.4 | Ex Vivo Studies

2.4.1 | Animals and Brain Preparation

Male Wistar rats (150–200 g) were obtained from the Department of Biochemistry. The brain tissue was prepared according to the protocol described by O. A. Ojo et al. (2024).

2.4.2 | Induction of Brain Injury ex Vivo

Brain damage was induced ex vivo via the addition of Fe^{2+} following the methods described by Erukainure et al. (2020) and O. A. Ojo et al. (2024).

2.4.3 | Evaluation of Monoamine Oxidase (MAO) Activity

The monoamine oxidase (MAO) activity was evaluated via the procedure described by Green and Haughton (1961).

2.5 | HPLC–DAD Analysis of Flavonoid-Rich Extracts of *B. vulgaris* Leaves

Flavonoid-rich extracts of *B. vulgaris* were subjected to HPLC to identify the potential bioactive flavonoids present. The procedure described in a previously published article was followed for this process (Araujo-León et al. 2019; O. A. Ojo et al. 2024).

2.6 | Molecular Docking Studies of Target Compounds From Flavonoid-Rich Extracts of *B. vulgaris* Leaves Identified by HPLC

2.6.1 | Protein Structure Preparation

Protein structures for human α-amylase-acarbose (PDB ID: 1B2Y), α-glucosidase-acarbose (PDB ID: 3TOP), acetylcholinesterase-donepezil (PDB ID: 4EY7), butyrylcholinesterase-decamethonium (PDB ID: 6EP4), and monoamine oxidase B-safinamide (PDB ID: 2V5Z) were retrieved from the Protein Data Bank.

(http://www.rcsb.org) selected the active site regions on the basis of their high-resolution quality and completeness. To prepare these structures for molecular docking, standard structural optimization procedures were applied, which included the removal of existing ligands and water molecules, and missing hydrogen atoms were added via MGL-AutoDockTools (ADT, v1.5.6) (Morris et al. 2009). As the structures were of high quality with no significant missing regions, homology modeling was not needed. This optimization ensured accurate docking interactions and reliable simulation outcomes.

2.6.2 | Ligand Preparation

The structural data (SDF) of reference inhibitors (donepezil, galantamine, decamethonium acarbose and safinamide) and the ligand compounds of *Syzygium aromaticum* were downloaded from www.pubchem.ncbi.nlm.nih.gov. The ligands were then converted to the pdb format via Open Babel.

2.6.3 | Validation of the Molecular Docking Studies

Molecular docking studies were validated following the detailed procedure described by O. A. Ojo et al. (2024).

2.6.4 | Molecular Docking of Phytochemicals With Targeted Active Sites

The reference inhibitors and the ligands were docked at the active site against the five protein targets via AutoDock Vina version 1.1.2 in PyRx 0.8 (Trott and Olson 2010). The default parameters of AutoDock Vina were employed, including an exhaustiveness of 8. PyRx 0.8's Open Babel 2.3.2 version, which employs its default force field (O'Boyle 2011), was used to minimize energy. The grid box dimensions for each protein target were meticulously defined to encompass the entire active site, ensuring comprehensive sampling of potential binding poses; the binding site coordinates are presented in Supporting Information S1: Table S1.

2.6.5 | Molecular Dynamics

Molecular dynamics simulation at 100 ns was performed for the hit compounds with 4EY7 and 1B2Y. This was achieved via the GROMACS 2019.2 and GROMOS96 43a1 force fields (O. A. Ojo et al. 2024). The protein and ligand topology files were generated via Charmm GUI (Lee et al. 2016, 2020). The enzymes and ligand–enzyme complex systems were immersed in a cubic box using the TIP4P water model, with periodic boundary conditions applied. The system was set to a physiological concentration of 0.154 M and maintained with neutralized NaCl ions. For α-amylase (PDB ID: 1B2Y), the grid box was centered around the carbohydrate-binding pocket, with adjustments made to better accommodate its extended hydrophilic cleft. For acetylcholinesterase (PDB ID: 4EY7), the grid was repositioned to encompass the aromatic-rich gorge region, and the side-chain flexibility of key active site residues was considered to better mimic native ligand interactions. These targeted optimizations allowed the docking simulations to more accurately reflect the unique structural and chemical environments of each enzyme's active site. On the basis of previous research studies, the parameters employed are as described previously (Ogunyemi et al. 2023; Gyebi et al. 2021; Ogunyemi et al. 2021; O. A. Ojo et al. 2024).

2.6.6 | Binding Free Energy Calculation Via MM-GBSA

The binding free energies of the top two phytochemicals were calculated via MM-GBSA implemented in the gmx MMPBSA package (Valdés-Tresanco et al. 2021; Miller III et al. 2012). Per-residue decomposition analysis was performed for residues within 0.5 nm of the ligand, following our established methods (Gyebi et al. 2021; O. A. Ojo et al. 2024).

2.7 | Data Analysis

The data are presented as the means ± SDs ($n = 3$). One-way ANOVA followed by Tukey's multiple comparison test was used to determine statistical significance ($p < 0.05$). Graphs were generated via GraphPad Prism version 9.0.

3 | Results

3.1 | Inhibition of α-Amylase and α-Glucosidase Enzymes

Inhibiting α-amylase and α-glucosidase enzymes significantly delays starch hydrolysis into sugars, thereby lowering blood glucose levels and rendering enzyme inhibitors potential candidates for antidiabetic therapy. Figure 1A and 2 illustrate the percentage inhibitory effects of various extracts against these enzymes at different concentrations. In particular, the flavonoid-rich extract of *B. vulgaris* leaves exhibited considerable ($p < 0.0001$) α-amylase inhibitory activity ($p < 0.0001$), with an IC_{50} of 102.808 ± 3.153 µg/mL, albeit weaker than that of the established starch blocker acarbose, with an IC_{50} of 27.104 ± 0.270 µg/mL (Figure 1B). Furthermore, the flavonoid-

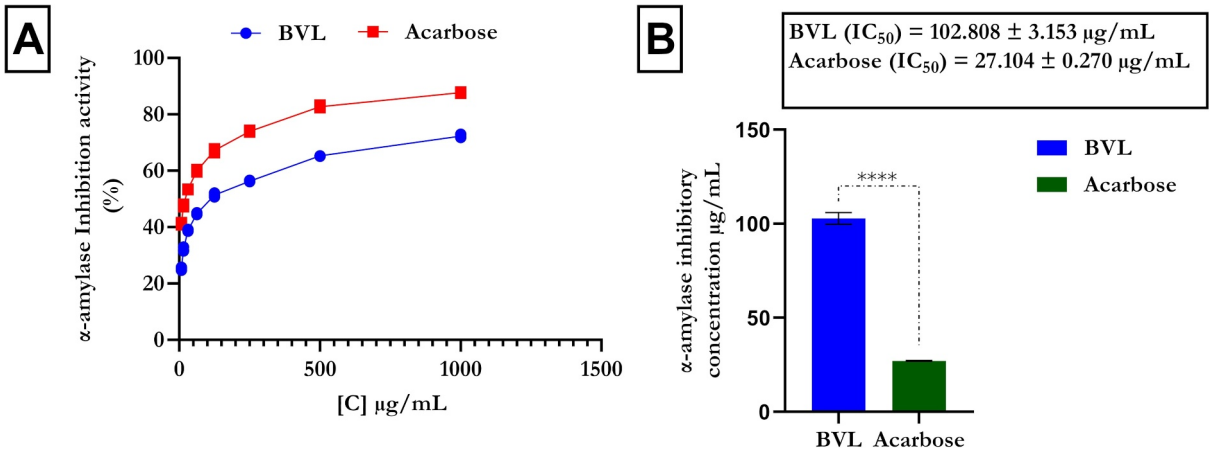

FIGURE 1 | α-Amylase inhibitory activity of *Beta vulgaris* leaf flavonoid-rich extracts: (A) α-amylase percentage inhibitory activity; (B) inhibitory concentration (IC_{50}) values of BVL and acarbose. Data are represented as the mean ± SD ($n = 3$); ****$p < 0.0001$ indicates an extremely significant difference compared with the standard drug (acarbose). Acarbose, standard drug; BVL, *B. vulgaris* leaf.

rich extract of *B. vulgaris* leaves inhibited α-glucosidase in a concentration-dependent manner, with an IC50 of 79.131 ± 1.129 μg/mL, in contrast to the IC50 of acarbose (17.389 ± 0.436 μg/mL) for acarbose (Figure 2A,B).

3.2 | Acetylcholinesterase and Butyrylcholinesterase Inhibitory Activity

The potential of the flavonoid-rich *B. vulgaris* leaf extract to inhibit acetylcholinesterase (AChE) and butyrylcholinesterase (BChE), key enzymes involved in neurotransmitter regulation, was evaluated. Figures 3 and 4 illustrate the dose-dependent inhibitory effects on both enzymes. The extract moderately inhibited AChE (IC_{50} = 902.738 ± 1.199 μg/mL, $p < 0.0001$) and BChE (IC_{50} = 143.742 ± 0.785 μg/mL, $p < 0.0001$), although less potently than the standard control, galantamine (IC_{50} = 27.950 ± 0.122 μg/mL for AChE) and (IC_{50} = 23.126 ± 0.683 μg/mL for BChE) (Table 1).

3.3 | Monoamine Oxidase Activity

Figure 5 illustrates the inhibitory effects of flavonoid-rich extracts on MAO activity in oxidized brain tissue. Untreated rats presented significantly increased MAO activity ($p < 0.0001$). Treatment with various doses of *B. vulgaris* leaf extract resulted in a significant decrease in MAO activity ($p < 0.0001$). The inhibitory effect was concentration dependent, with the greatest inhibition observed at 1000 μg/mL.

3.4 | HPLC–DAD Analysis of Flavonoid-Rich Extracts of *B. vulgaris* Leaves

Chromatograms obtained at different retention times from HPLC-DAD analysis of the flavonoid-rich extract of *B. vulgaris* leaves (Supporting Information S1: Figure S1) revealed several constituents: gallic acid, caffeic acid, syringic acid, rutin, myricetin, apigenin, and kaempferol (Table 2).

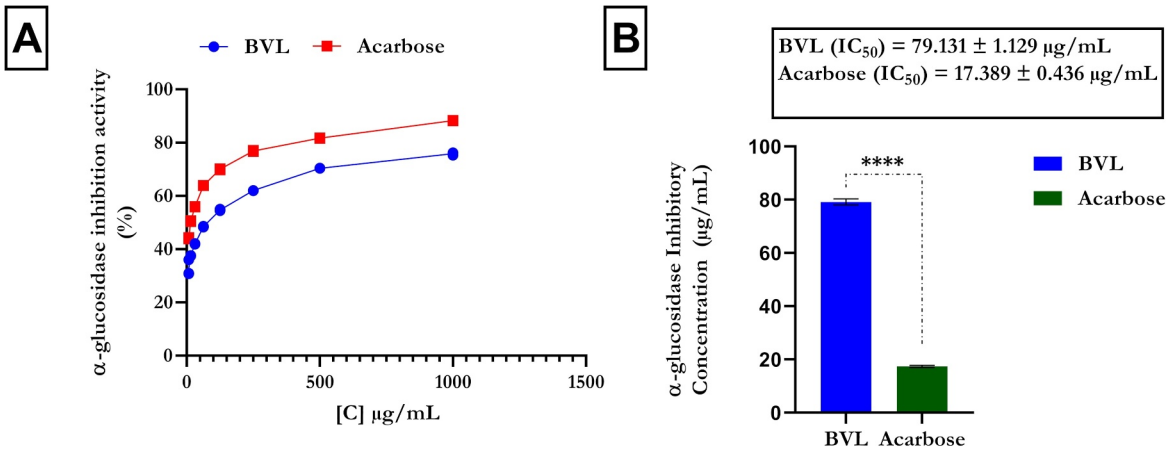

FIGURE 2 | α-Glucosidase inhibitory activity of *B. vulgaris* leaf flavonoid-rich extracts: (A) α-glucosidase percentage inhibitory activity; (B) inhibitory concentration (IC_{50}) values of BVL and acarbose. Data are represented as the mean ± SD (n = 3); ****$p < 0.0001$ indicates an extremely significant difference compared with the standard drug (acarbose). Acarbose, standard drug; BVL, *B. vulgaris* leaf.

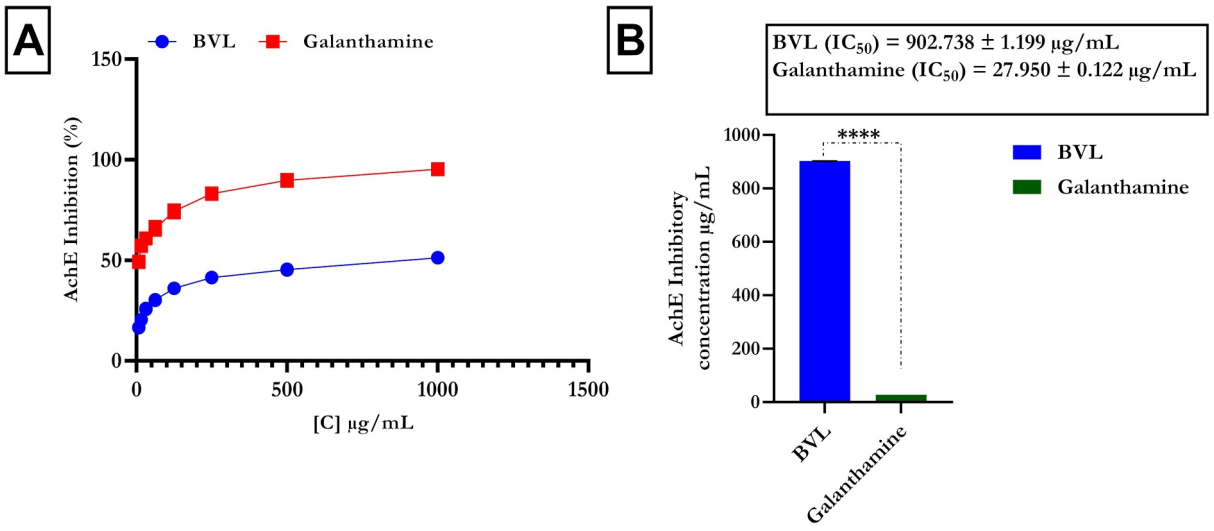

FIGURE 3 | Acetylcholinesterase activity of *B. vulgaris* leaf flavonoid-rich extracts: (A) AchE percentage inhibitory activity and (B) inhibitory concentration (IC_{50}) values of BVL and galanthamine. Data are represented as the mean ± SD (n = 3); ****$p < 0.0001$ indicates an extremely significant difference compared with the standard drug (galanthamine). BVL, *B. vulgaris* leaf; galanthamine, standard drug.

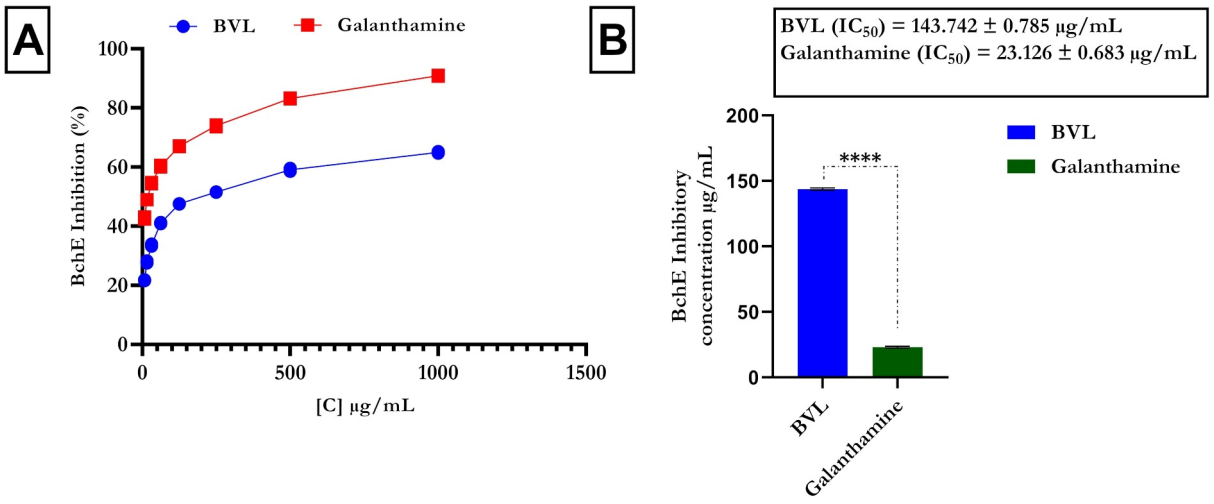

FIGURE 4 | Butyrylcholinesterase activity of *B. vulgaris* leaf flavonoid-rich extracts: (A) BchE percentage inhibitory activity and (B) inhibitory concentration (IC_{50}) values of BVL and galanthamine. Data are represented as the mean ± SD ($n = 3$); ****$p < 0.0001$ indicates an extremely significant difference compared with the standard drug (galanthamine). BVL, *B. vulgaris* leaf; galanthamine, standard drug.

TABLE 1 | Binding energies of HPLC-identified compounds from flavonoid-rich extracts of *Beta vulgaris* leaves against target proteins.

	Binding affinity				
Ligand	**1B2Y**	**3TOP**	**4EY7**	**6EP4**	**2V5Z**
Donepezil (uff_*E* = 306.68)			−12.2	−9.6	−11.1
Decamethonium (uff_*E* = 261.56)			−6.8	−5.4	−6.2
Acarbose_3top (uff_*E* = 372.76)	−12.5	−14.2			
Safinamide (uff_*E* = 122.72)					−9.8
Rutin (uff_*E* = 751.29)	−8.9	−8.8	−9.4	−10.6	−7.5
Myricetin_uff_*E* = 388.24)	−9.1	−8.8	−10.1	−9.5	−9.3
Apigenin (uff_*E* = 233.26)	−9	−9.1	−10.2	−9.3	−9.4
Kaempferol (uff_*E* = 362.50)	−8.8	−8.7	−9.3	−9.3	−9.2
Caffeic_acid (uff_*E* = 98.70)	−6.6	−6.9	−7.7	−6.8	−7.3
Gallic_acid (uff_*E* = 77.81)	−6.2	−6.4	−6.6	−6	−6.3
Syringic_acid (uff_*E* = 109.99)	−5.7	−6.1	−6.6	−5.9	−6.3

3.5 | Molecular Docking Studies

3.5.1 | Molecular Docking of HPLC-Identified Compounds From Flavonoid-Rich Extracts of *B. vulgaris* Leaves Against Target Proteins

Table 1 presents the binding affinities of the identified compounds against five protein targets. The top two compounds with the lowest binding energies and favorable interactions within the catalytic site were selected for further analysis. Notably, these top two compounds presented binding energies closely resembling those of the reference inhibitors (as indicated in Table 1). To validate the docking protocol, cocrystallized reference compounds (donepezil and acarbose) were docked into their respective protein binding sites, yielding binding energies of −12.2 and −12.5 kcal/mol, respectively (Supporting Information S1: Figure S2). To validate the docking scores, cocrystalized reference compounds (donepezil and acarbose) were docked into the binding site of the cocrystalized proteins with binding energies of −12.2 and −12.5 kcal/mol, respectively (Supporting Information S1: Figure S2). With the exception of the 6EP4 targets, where rutin and myricetin were the top docked compounds with binding energies of −10.6 and −9.5, respectively, apigenin and myricetin demonstrated the highest binding tendencies (−9.1 and −8.8, −9 and −9.1, −10.2 and −10.1, and −9.4 and −9.3, respectively, to the remaining protein targets (3top, 1b2y, 4ey7 and 2v5z)) (Supporting Information S1: Table S2).

3.5.2 | Interactions of Amino Acids With the Top Two Docked HPLC-Identified Phytochemicals From Flavonoid-Rich Extracts of *B. vulgaris* Leaves and Reference Compounds With Five Protein Targets

Table 3 summarizes the interactions between the reference compounds and the top-scoring ligands with the catalytic residues of the target proteins. Most interactions are hydrophobic,

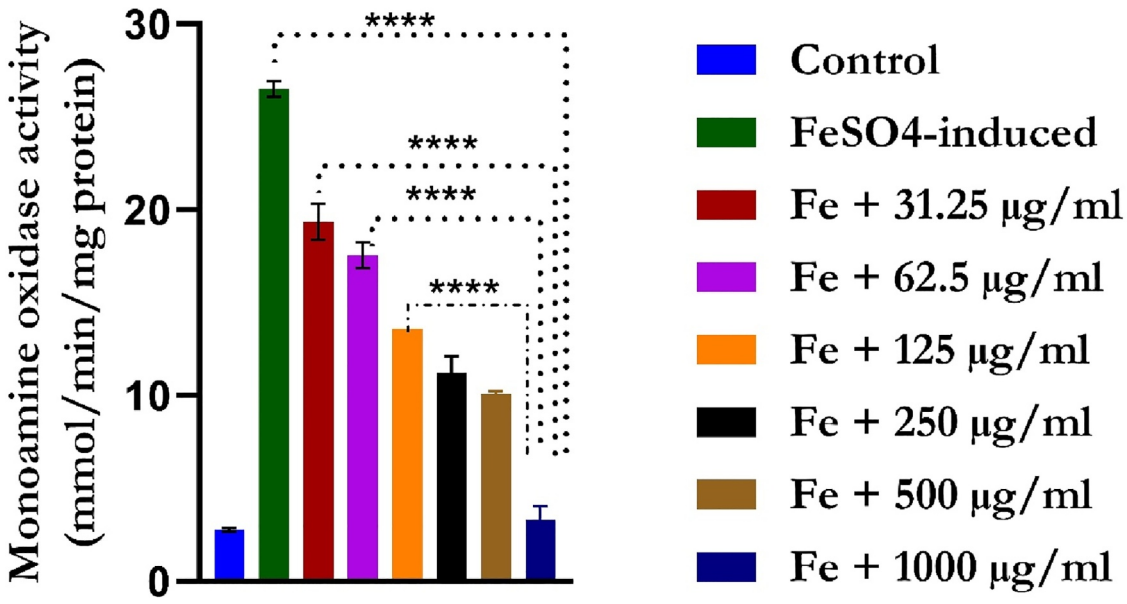

FIGURE 5 | Effects of varying concentrations of *B. vulgaris* leaf flavonoid-rich extracts on monoamine oxidase (MAO) activity in ex vivo brain samples. Compared with the group induced solely with FeSO4, a notable reduction in MAO activity was observed in the range of flavonoid-rich extracts of *B. vulgaris* leaf concentrations. Data are represented as the mean ± SD ($n = 3$); ****$p < 0.0001$ indicates an extremely significant difference compared with the control. BVL, *B. vulgaris* leaf.

TABLE 2 | Bioactive principles identified in flavonoid-rich extracts of *B. vulgaris* leaves.

Compounds	Retention time
Gallic acid	3.066
Caffeic acid	2.068
Syringic acid	3.544
Rutin	4.814
Myricetin	7.484
Apigenin	13.046
Kaempferol	16.355

with few hydrogen bonds. Donepezil formed a single hydrogen bond with Phe295 and multiple pi-pi and pi-alkyl interactions with Tyr337, Tyr341, Trp86, His447, Trp286, and Phe338. Apigenin and myricetin, the top-scoring ligands for 4EY7, adopt a similar binding orientation, forming multiple hydrogen bonds and hydrophobic contacts (Figure 6). Decamethonium, the reference compound for 6EP4, was deeply docked into the active site gorge. Although they formed no hydrogen bonds, the top-scoring ligands (rutin and myricetin) formed multiple hydrogen bonds with the catalytic residues, mimicking the interactions of decamethonium (Figure 7). For 1B2Y, acarbose occupied all five subsites, whereas apigenin and myricetin primarily targeted the −3 and −1 subsites (Figure 8). Both phytochemicals interact with catalytic residues, such as Trp-59, Tyr62, His299, Asp197, His305, Glu233, Arg197, and Ala198. For 3TOP, apigenin and myricetin adopt a similar binding mode to acarbose, interacting with catalytic residues within the active site (Figure 9). In contrast, safinamide formed only one hydrogen bond with Gln206 and several hydrophobic interactions. The top-scoring ligands established additional hydrogen bonds with the catalytic residues, enhancing their interactions (Figure 10).

3.5.3 | Molecular Dynamics Simulation

We assessed the stability of complexes, including representative proteins and reference inhibitors (acarbose and donepezil), during the molecular dynamics phase via Tk console scripts. The MD trajectories were analyzed via RMSD (root mean square deviation), RMSF (root mean square fluctuation), RoG (radius of gyration), SASA (solvent-accessible surface area), and the number of hydrogen bonds. Table 4 summarizes the averages and standard deviations of these parameters, whereas Supporting Information S1: Figures S3–S6 depict the intricate spectrum plots. Specifically, the RMSD plots for the 4EY7 and 1B2Y complexes reached equilibrium before 10 ns, exhibiting minimal fluctuations throughout the remaining simulation period (Supporting Information S1: Figure S3). Notably, 4EY7_Apigenin and 1B2Y_Apigenin displayed the greatest fluctuations in mean RMSD values. For the 4EY7 systems, the three variants presented closely matched mean RMSF values, and the 1B2Y complex exhibited similar behavior (Supporting Information S1: Figure S4). RoG plots indicated that both the 4EY7 and 1B2Y complexes reached equilibrium at approximately 10 ns, maintaining stability throughout the simulation (Supporting Information S1: Figure S5). The RoG values for apigenin, myricetin, and the reference compounds were comparable. SASA plots (Supporting Information S1: Figure S6) and mean SASA values confirmed minimal fluctuations in solvent accessibility during the simulation. Additionally, the number of hydrogen bonds remained stable, with minimal variation across the ligand-bound complexes (Supporting Information S1: Figure S7).

TABLE 3 | Amino acid interactions of the top two docked high-performance liquid chromatography (HPLC)-identified phytochemicals from the docking analysis of the five target proteins.

		Hydrogen bonds	Hydrophobic interaction
Compounds	**Protein**	**Interacting residues**	**Interacting residues**
Donepezil	4EY7	Phe295	Trp86 Phe338 His447 Tyr337 Tyr341 Trp286 Tyr72 Leu289
Apigenin		Tyr341 Ser293 Gly122 Ser203 His447 Ala204	Trp286 Phe297 Tyr341 Phe338
Myricetin		Ser293 Tyr341 Phe295 Phe338 Tyr124	Tyr72 Trp286 Val294 Tyr341
Decamethonium	6EP4		Asp70 His438 Trp82
Myricetin		His438 Tyr332 Asn83 Gln67 Asp70 Asn68 Thr120 Trp82 Glu197 Gly115 Tyr128	Trp82 His438 Asp70
Rutin		Als328 Trp82 Tyr440 His438 Thr284 Tyr332 Gly78 Asp70 Ser79 As83 Pro285 Thr120 Ala199 Gly117 Ser198 Gln119	Phe329 Thr284 Asp70 Ala328
Acarbose	1B2Y	Trp59 Gln63 Tyr62 Thr163 GLy306 Thr163 His305 His299 Tyr62 Tyr151 His201 Lys200 Ile235 Arg195 Asp197 Lys200 Glu233 Asp300	Trp59
Myricetin		Gln63 Tyr62 His101 Asp300 His299 Arg195 Ala198 Asp197 Glu233	Trp59 Tyr62 Asp197
Apigenin		Gln63 Asp300 His299 Asp197 His305 Arg195 Glu233	Trp59 Tyr62
Acarbose	3top	Asp1555 Arg1582 Asp1317 His1584 Trp1355 Thr1528 Gln1561 Lys1460 Asp1157 Met1421 Tyr1167 Arg1516 Asp1526	Tyr1251 Phe1559
Apigenin		Asp1157 Lys1460 Arg1510 His1584 Asp1279 Thr1586 Trp1369	Phe1560 Trp1355 Tyr1251 Pro1159
Myricetin		Trp1369 Asp1157 Lys1460 Asp1279 His1584 Ile1587 Asp1420 Asp1526 Thr1586 Arg1510	Trp1369 Trp1355 Phe1559 Phe1560 Asp1526
Safinamide	2V5Z	Gln206	Tyr398 Tyr326 Leu171 Ile199 Ile316 Cys172
Apigenin		Gly57 Tyr188 Gly434 Ile199	Tyr398 Leu171
Myricetin		Cys172 Tyr435 Tyr188 Tyr60 Gly434 Ser59	Leu171 Tyr398 Tyr326 Ile198

3.5.4 | Molecular Mechanics Generalized Born Surface Area (MMGBSA) Analysis

Compared with the reference compounds, myricetin and apigenin presented the highest binding affinities for 4EY7 and 1B2Y, respectively. Table 5 summarizes the individual energy components contributing to the total binding free energy. Decomposition analysis (Figures S8-S9) revealed that the residues involved in the initial docking interactions were the primary contributors to the total binding energy.

4 | Discussion

Type 2 diabetes (T2D) and Alzheimer's disease (AD) are major health concerns worldwide. The number of people affected by these conditions is increasing, leading to extensive research on finding new treatments. Although they are often seen as diseases of advanced age, T2D and AD share common genetic factors and similar changes in the body; T2D affects pancreatic cells, and AD affects the brain. Despite many studies, we still do not fully understand how T2D and AD are connected, but there is evidence that having T2D increases the risk of developing AD (Sun et al. 2020; Hardy et al. 2022; Lynn et al. 2022). Both T2D and AD have several common characteristics, including insulin resistance, cardiovascular comorbidities, dyslipidemia, advanced glycation end-product formation, oxidative stress, vascular abnormalities, aberrant protein processing, and inflammatory pathway activation (Sun et al. 2020; Hardy et al. 2022). In AD, these factors contribute to the progressive decline in cognitive function and memory loss. The brain develops clumps of amyloid-beta (Aβ) protein, twisted strands of tau protein called neurofibrillary tangles, and experiences damage to neurons and connections between them in regions such as the hippocampus and cortex. On the other hand, T2D is characterized by insufficient insulin production by pancreatic beta cells and a reduced response of the body to insulin. Initially, the body compensates for this by producing more insulin, but over time, beta cell function decreases further, leading to high blood sugar levels and the onset of T2D. Notably, insulin also plays a role in the production of the Aβ protein in the brain, which is crucial for the development of AD (Wang et al. 2021; Richter et al. 2023).

Although various treatments are available for managing T2D and AD, researchers are actively looking for natural compounds that can be more effective with fewer side effects. An area of interest is medicinal plants that have shown potential in

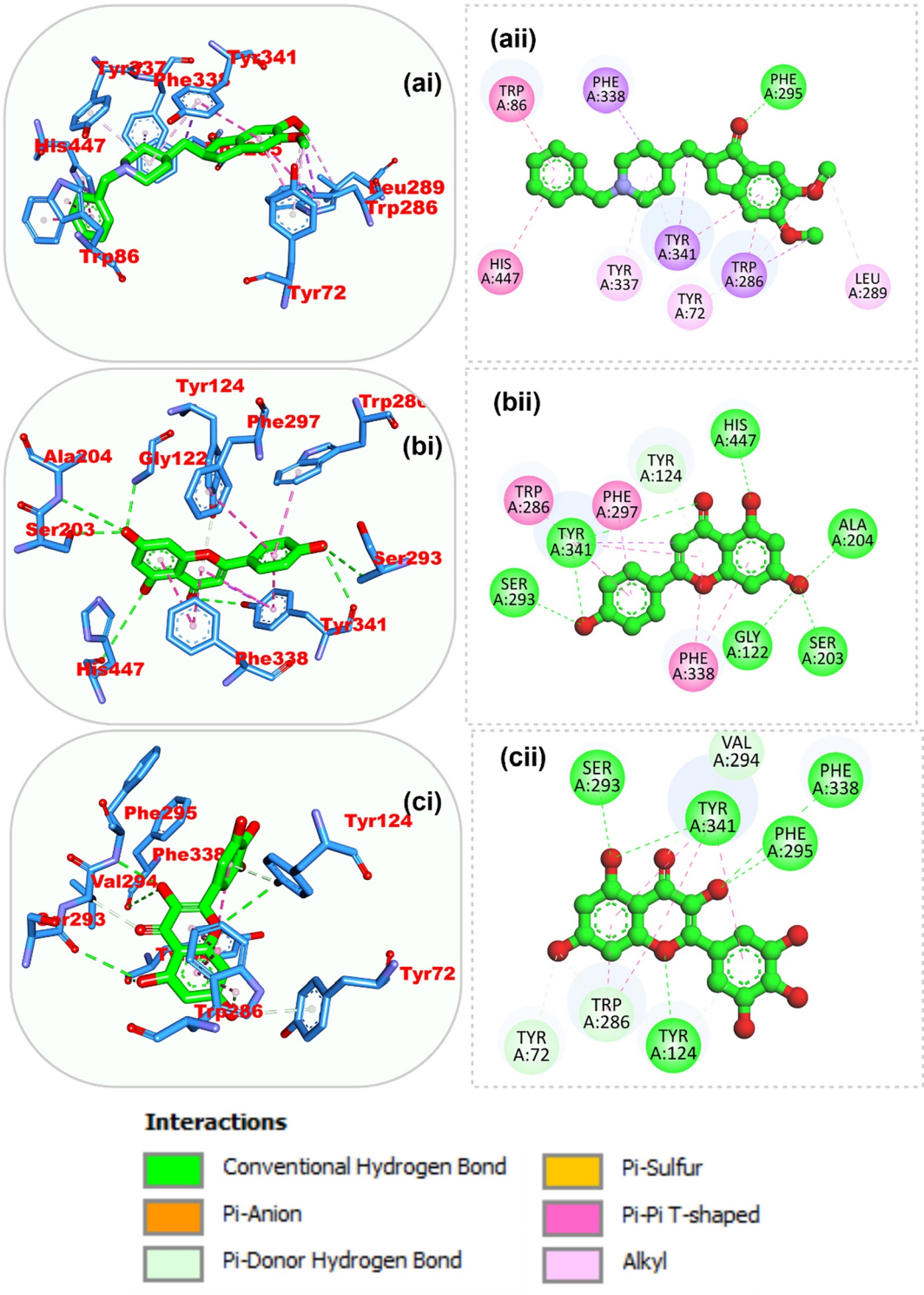

FIGURE 6 | Interactions of top-scoring ligands (apigenin and myricetin) and an acetylcholinesterase inhibitor (donepezil) within the active site of protein 4EY7. This figure illustrates the binding interactions of the reference inhibitor donepezil and the test ligands apigenin and myricetin within the active site of human acetylcholinesterase (AChE). Panels (a), (b), and (c) represent the ligands donepezil, apigenin, and myricetin, respectively, each shown in (i) The 3D binding pose shows its precise orientation and position within the enzyme's active site, highlighting key residues involved in hydrogen bonding, hydrophobic interactions, and other noncovalent forces. This view provides insight into the spatial complementarity between the ligand and the binding pocket. (ii) The 2D interaction representation details the specific amino acid residues of 4EY7 that form direct interactions with the ligand, along with the types of interactions (e.g., hydrogen bonds, pi–pi stacking, and van der Waals forces). This comprehensive visualization allows for a clear understanding of the molecular basis of ligand–enzyme recognition and provides crucial information for structure–activity relationship studies and future drug design efforts.

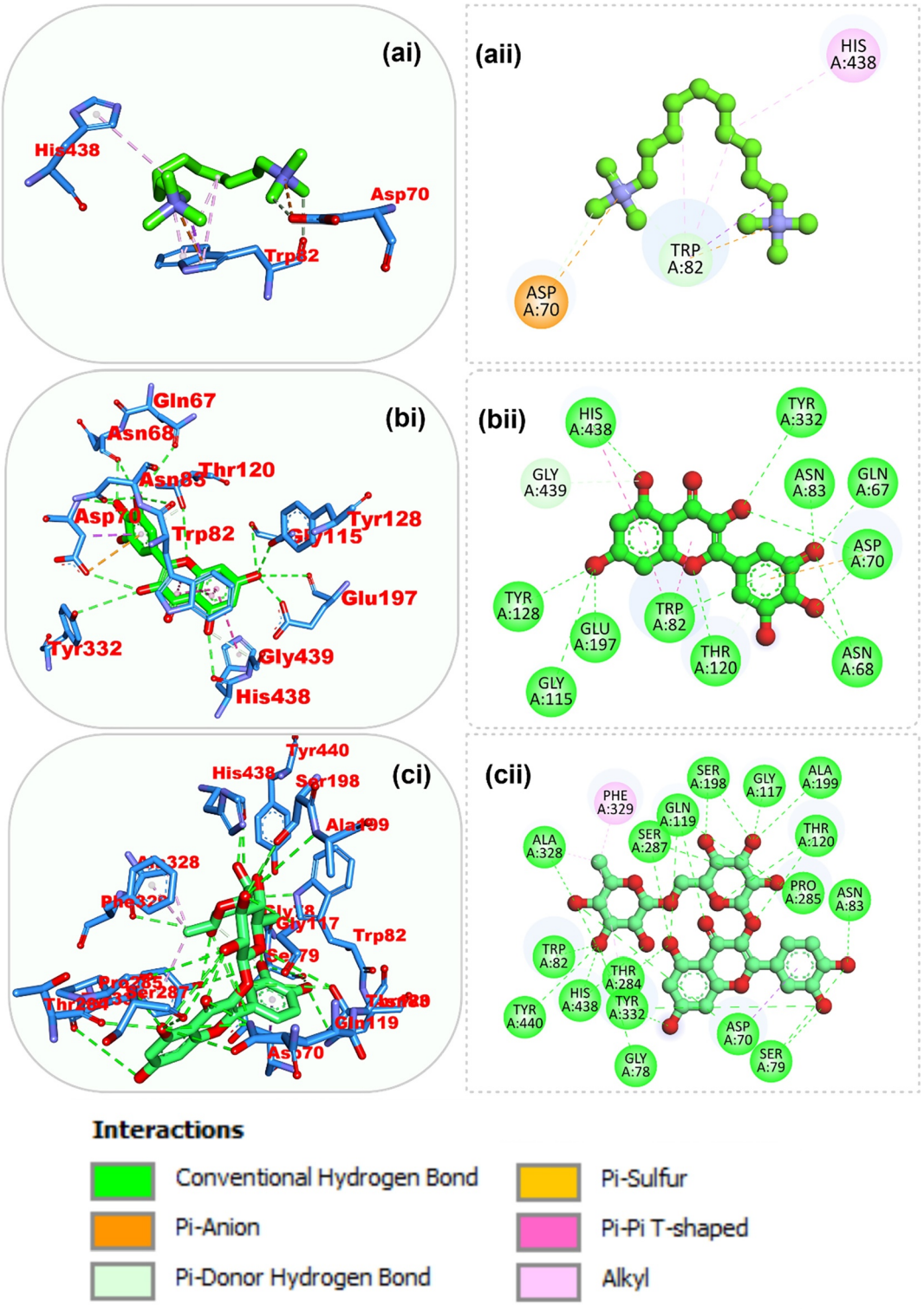

FIGURE 7 | Top scoring ligands (myricetin and rutin) and butylcholinestarse inhibitor (decamethonium) within the active site of protein 6EP4. This figure illustrates the binding interactions of the reference inhibitor decamethonium and the test ligands myricetin and rutin within the active site of human butylcholinesterase (BChE). Panels (a), (b), and (c) represent the ligands decamethonium, myricetin, and rutin, respectively, as shown in (i) The 3D binding pose shows its precise orientation and position within the enzyme's active site, highlighting key residues involved in hydrogen bonding, hydrophobic interactions, and other noncovalent forces. This view provides insight into the spatial complementarity between the ligand and the binding pocket. (ii) The 2D interaction representation details the specific amino acid residues of 6EP4 that form direct interactions with the ligand, along with the types of interactions (e.g., hydrogen bonds, pi–pi stacking, and van der Waals forces). This comprehensive visualization allows for a clear understanding of the molecular basis of ligand–enzyme recognition and provides crucial information for structure–activity relationship studies and future drug design efforts.

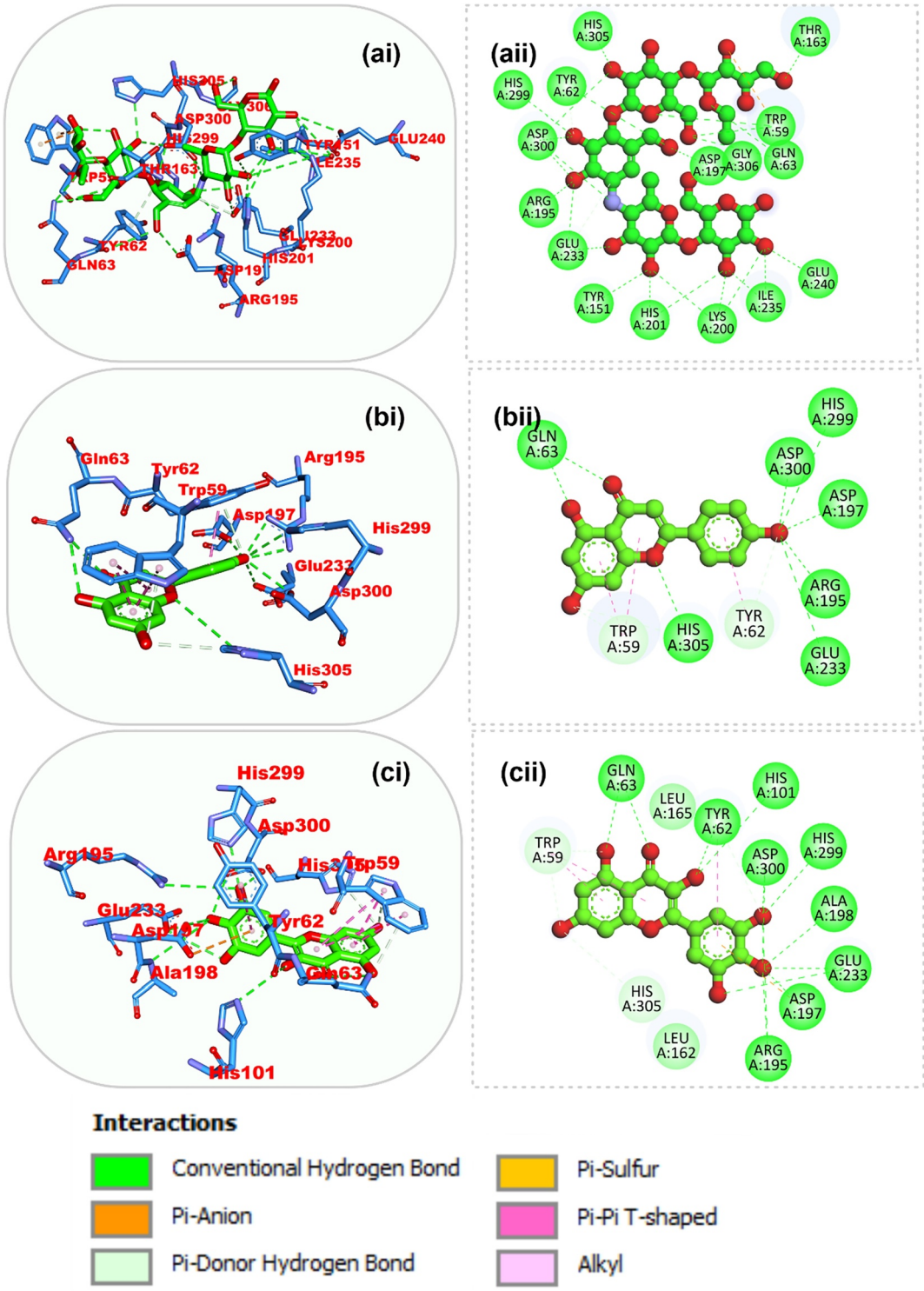

FIGURE 8 | Interactions of ligands (apigenin and myricetin) with the α-amylase inhibitor acarbose within the active site of protein 1B2Y. This figure illustrates the binding interactions of the reference inhibitor acarbose and the test ligands apigenin and myricetin within the active site of α-amylase. Panels (a), (b), and (c) represent the ligands acarbose, apigenin, and myricetin, respectively, each shown in (i) 3D binding pose showing its precise orientation and position within the enzyme's active site, highlighting key residues involved in hydrogen bonding, hydrophobic interactions, and other noncovalent forces. This view provides insight into the spatial complementarity between the ligand and the binding pocket. (ii) The 2D interaction representation details the specific amino acid residues of 1B2Y that form direct interactions with the ligand, along with the types of interactions (e.g., hydrogen bonds, pi–pi stacking, and van der Waals forces). This comprehensive visualization allows for a clear understanding of the molecular basis of ligand–enzyme recognition and provides crucial information for structure–activity relationship studies and future drug design efforts.

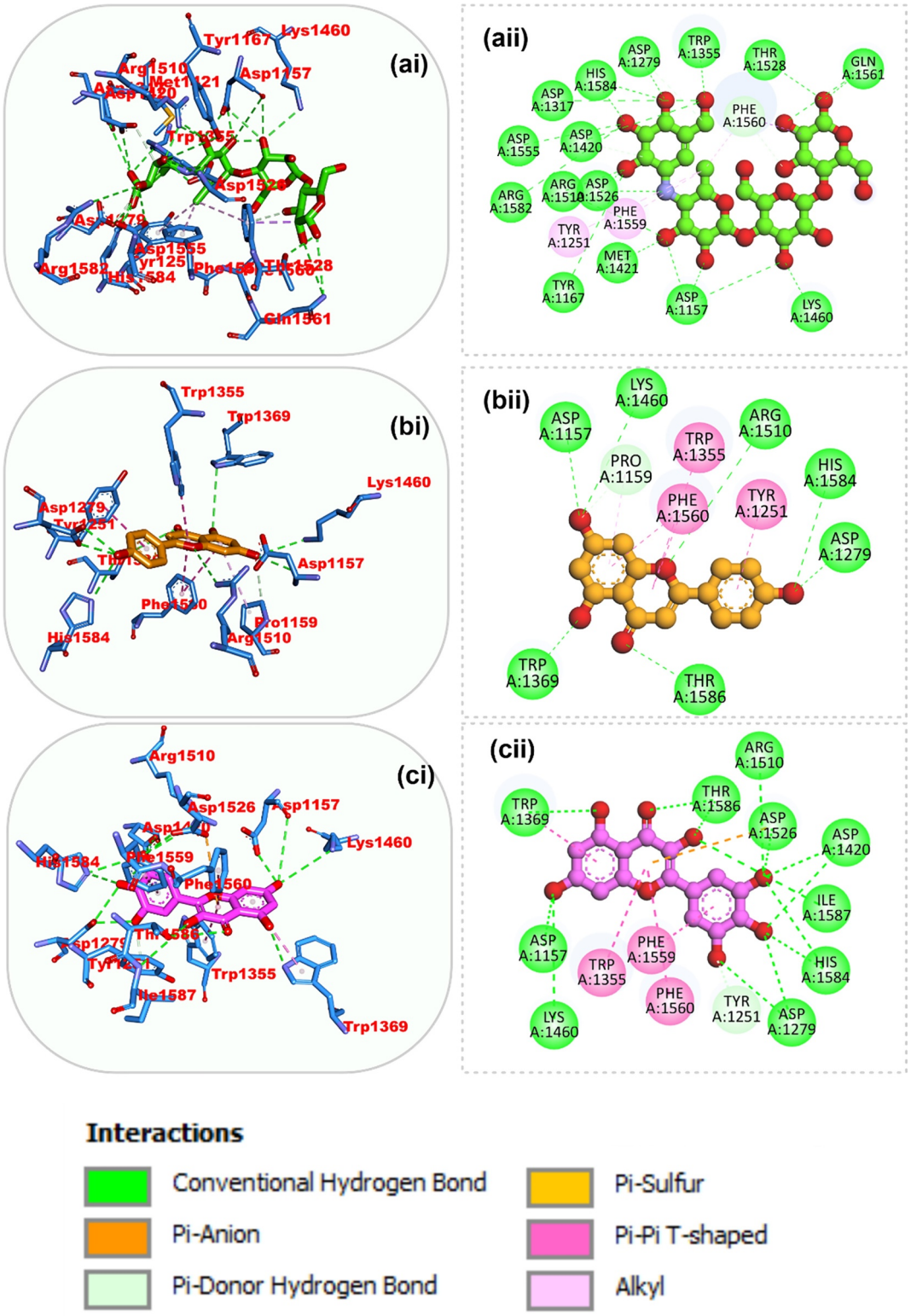

FIGURE 9 | Top scoring ligands (apigenin and myricetin) and an α-glucosidase inhibitor (acarbose) within the active site of the 3TOP protein. This figure illustrates the binding interactions of the reference inhibitor acarbose and the test ligands apigenin and myricetin within the active site of α-glucosidase. Panels (a), (b), and (c) represent the ligands acarbose, apigenin, and myricetin, respectively, each shown in (i) 3D binding pose showing its precise orientation and position within the enzyme's active site, highlighting key residues involved in hydrogen bonding, hydrophobic interactions, and other noncovalent forces. This view provides insight into the spatial complementarity between the ligand and the binding pocket. (ii) The 2D interaction representation details the specific amino acid residues of 3TOP that form direct interactions with the ligand, along with the types of interactions (e.g., hydrogen bonds, pi–pi stacking, and van der Waals forces). This comprehensive visualization allows for a clear understanding of the molecular basis of ligand–enzyme recognition and provides crucial information for structure–activity relationship studies and future drug design efforts.

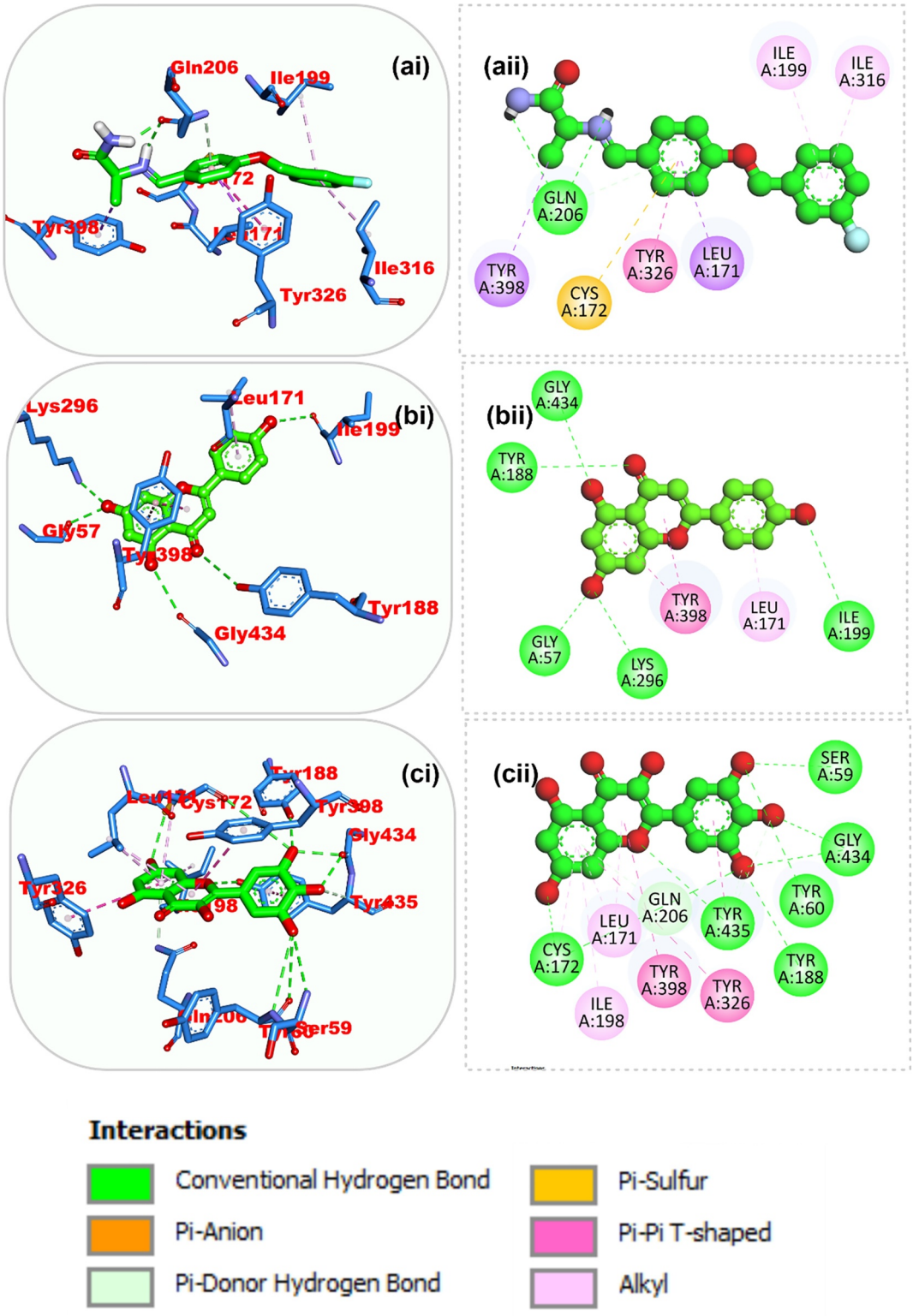

FIGURE 10 | Amino acid interactions of the top scoring ligands (apigenin and myricetin) and monoamine oxidase inhibitor (safinamide) within the active site of protein 2V5Z. This figure illustrates the binding interactions of the reference inhibitor safinamide and the test ligands apigenin and myricetin within the active site of monoamine oxidase (MAO). Panels (a), (b), and (c) represent the ligands safinamide, apigenin, and myricetin, respectively, each shown in (i) 3D binding pose showing its precise orientation and position within the enzyme's active site, highlighting key residues involved in hydrogen bonding, hydrophobic interactions, and other noncovalent forces. This view provides insight into the spatial complementarity between the ligand and the binding pocket. (ii) The 2D interaction representation details the specific amino acid residues of 2V5Z that form direct interactions with the ligand, along with the types of interactions (e.g., hydrogen bonds, pi–pi stacking, and van der Waals forces). This comprehensive visualization allows for a clear understanding of the molecular basis of ligand–enzyme recognition and provides crucial information for structure–activity relationship studies and future drug design efforts.

TABLE 4 | The means and standard deviations of different parameters analyzed from the MDS trajectories of the top docked compounds complexed with their respective targets.

	RMSD Mean (Å)	RMSF Mean(Å)	RoG Mean (Å)	SASA Mean (Å)	H-bonds Mean (Å)
4EY7_Donepezil	1.69 ± 0.23	0.86 ± 0.70	23.10 ± 0.10	23046.95 ± 465.99	114.29 ± 9.23
4EY7_Apigenin	1.75 ± 0.26	0.80 ± 0.49	23.14 ± 0.08	23041.45 ± 419.53	115.60 ± 8.71
4EY7_Myricetin	1.71 ± 0.22	0.83 ± 0.54	23.12 ± 0.08	23146.39 ± 487.86	114.23 ± 9.31
1B2Y_ Acarbose	1.53 ± 0.25	0.95 ± 0.53	23.33 ± 0.08	21387.142 ± 438.87	121.71 ± 9.37
1B2Y_Apigenin	1.70 ± 0.22	0.80 ± 0.48	23.26 ± 0.07	21166.23 ± 286.37	126.08 ± 8.55
1B2Y_Myricetin	1.53 ± 0.21	0.84 ± 0.46	23.34 ± 0.09	21155.54 ± 361.45	123.78 ± 9.02

TABLE 5 | Means and SDs of different energy components that determine the binding free energies of the top docked phytochemicals to target proteins.

System	$\Delta_{VDWAALS}$	Δ_{EEL}	Δ_{EGB}	Δ_{ESURF}	Δ_{GGAS}	Δ_{GSOLV}	Δ_{TOTAL}
4ey7_ Donepezil	−42.78 ± 3.08	−9.71 ± 11.53	38.59 ± 10.65	−5.99 ± 0.37	−52.49 ± 12.24	32.6 ± 10.5	−19.89 ± 3.61
4EY7_Apigenin	−31.28 ± 4.17	−15.09 ± 7.50	28.26 ± 5.26	−4.09 ± 0.53	−46.37 ± 9.34	24.18 ± 5.09	−22.19 ± 5.17
4EY7_Myricetin	−38.22 ± 3.73	−34.14 ± 10.24	51.66 ± 6.75	−5.08 ± 0.29	−72.36 ± 9.55	46.58 ± 6.65	−25.77 ± 4.03
1B2Y_ acarbose	−10.53 ± 8.67	−16.01 ± 20.79	18.47 ± 19.76	−2.25 ± 1.82	−26.54 ± 27.77	16.22 ± 18.05	−10.32 ± 10.61
1B2Y_Apigenin	−29.05 ± 2.74	−20.61 ± 5.48	34.03 ± 4.51	−3.77 ± 0.36	−49.66 ± 6.07	30.26 ± 4.29	−19.40 ± 2.76
1B2Y_Myricetin	−23.47 ± 4.97	−26.11 ± 15.01	35.05 ± 9.59	−3.13 ± 0.64	−49.58 ± 14.68	31.92 ± 9.28	−17.66 ± 6.00

preventing diseases. Specifically, scientists are studying plant-based compounds called flavonoids for their ability to improve various health conditions.

This investigation demonstrated the significant inhibitory effects of flavonoid-rich extracts of *B. vulgaris* leaves on α-glucosidase and α-amylase enzymatic activities, which are crucial for the regulation of postprandial hyperglycemia in individuals with type 2 diabetes mellitus (T2DM) (Egbuna et al. 2021). Flavonoids, known for their antioxidant properties, have been found to inhibit these enzymes. The presence of specific chemical groups in flavonoids appears to be responsible for this effect (Egbuna et al. 2021). These findings indicate that flavonoid-rich extracts of *B. vulgaris* leaves could be used as a natural treatment option for postprandial hyperglycemia in patients with T2DM. However, more research is needed to fully understand its effectiveness and safety. Overall, this study adds to the growing body of evidence supporting the use of natural compounds to prevent and manage chronic diseases such as T2D and AD.

Acetylcholinesterase (AChE) and butyrylcholinesterase (BChE) facilitate the degradation of acetylcholine, resulting in decreased neurotransmission levels and gradual cognitive decline. By impeding the activity of these enzymes, cholinergic transmission in the brain can be increased (Moreira et al. 2022; Chen et al. 2022). The present study revealed substantial inhibition of AChE and BChE by the flavonoid-rich extract of *B. vulgaris* leaves, suggesting its potential neuroprotective efficacy in the treatment of AD. In line with the therapeutic relevance of combination strategies, although FREBVL exhibited moderate inhibitory effects against α-amylase, α-glucosidase, and cholinesterase, its activities were lower than those of standard drugs such as acarbose and galantamine. This observation suggests that combining FREBVL with these reference compounds may offer enhanced efficacy through additive or synergistic interactions. Although such combination therapy experiments were not within the scope of the current study, they represent a promising avenue for future research aimed at improving the pharmacological profile and clinical applicability of FREBVL in managing metabolic and neurodegenerative disorders.

The inhibition of monoamine oxidase (MAO) is a key strategy in Alzheimer's disease treatment. Flavonoid-rich extracts from *B. vulgaris* leaves demonstrate MAO inhibitory potential, suggesting their therapeutic potential. This inhibition could increase the levels of neurotransmitters such as dopamine and serotonin while mitigating the oxidative stress induced by reactive oxygen species (ROS) (Chaurasiya et al. 2022).

The combination of "wet-lab" research and computational techniques results in better knowledge of the chemical interactions between several ligands and recognized receptors. These molecular interactions may provide further information for interpreting experimental data at the atomic level (Munsamy and Soliman 2019; O. A. Ojo, Agboola, et al. 2023). To predict the manner of interaction between a ligand and a receptor protein, computer-aided drug design uses structure-based screening techniques, which include molecular docking and molecular dynamics simulation studies (Santana Azevedo et al. 2012; O. A. Ojo, Ogunlakin, Gyebi, Ayokunle, Odugbemi, Babatunde, Akintunde, et al. 2023; O. A. Ojo, Ogunlakin, Gyebi, Ayokunle, Odugbemi, Babatunde, Ajayi-Odoko, et al. 2023). Potential inhibitors of a number of cholingenic and other neurotherapeutic targets derived from plant sources have been identified via these models (Silva et al. 2019; Falade et al. 2022). In this study, seven (7) bioactive compounds were identified from *B. vulgaris* leaves via HPLC-DAD. The compounds gallic acid, caffeic acid, syringic acid, rutin, myricetin,

apigenin and kaempferol were tested against five protein targets relevant to T2DM and AD, namely, α-amylase, α-glucosidase, AChE, BChE, and MAO. Reference protein targets (donepezil, deecamethonium, and acarbose) were compared with these targets. Apigenin, myricetin, and rutin were selected as lead drug candidates with high binding affinities for two or more targets.

The inhibitory effects of the flavonoid-rich extract of *B. vulgaris* leaves may be due to the presence of bioactive flavonoids in the plant. The exceptional inhibitory binding tendencies of these bioactive flavonoids may be explained by the numerous hydroxyl groups and oxygen atoms they have linked to their various structural frames. Numerous in vitro, in vivo, and in silico studies have demonstrated the antidiabetic and neuroprotective properties of these lead bioactive flavonoids through the inhibition of one or more targets examined in this work (Khan et al. 2018; Javaid et al. 2021; Oh et al., 2021; Abd El-Aziz et al. 2021; Sánchez-Martínez et al. 2021; Karimi et al. 2021). Thus, it can be inferred that the lead bioactive flavonoids, which showed various high binding affinities to the studied targets, may have contributed partially or cooperatively to the enzyme inhibitory activities (α-amylase, α-glucosidase, AchE, BchE, and MAO) of the flavonoid-rich extract.

To assess the stability of the protein–ligand complexes, 100 ns molecular dynamics simulations were performed. Analysis of key thermodynamic metrics (RMSD, RMSF, RoG, SAS, and H-bond number) indicated that the complexes maintained structural integrity throughout the simulation. On the basis of our findings, the mean RMSD values revealed that 4EY7_Apigenin and 1B2Y_Apigenin presented the greatest fluctuations. The 4EY7 systems exhibited similar RMSF profiles, indicating comparable protein flexibility. RoG, SASA, and H-bond analyses revealed that the 4EY7 and 1B2Y complexes were stable throughout the simulation period.

The lead bioactive flavonoids did not induce significant conformational changes in the protein structures. Instead, they formed more compact complexes, as evidenced by RMSF analysis (Dong et al. 2018; A. B. Ojo et al. 2022). The close mean values of various thermodynamic parameters for the ligand-bound and unbound proteins suggest that ligand binding did not compromise protein integrity (Dong et al. 2018; Gyebi et al. 2022). MM-GBSA calculations provided insights into the binding mechanisms of the top-ranked phytochemicals for the 4EY7 and 1B2Y proteins (Kollman et al. 2000).

5 | Conclusions

This study explored the potential of *B. vulgaris* leaf extract to inhibit enzymes linked to type 2 diabetes mellitus (T2DM) and Alzheimer's disease (AD). Bioactive compounds, including rutin, apigenin, and myricetin, were identified via HPLC. Computational studies, including in silico docking, revealed strong interactions between these compounds and key protein targets associated with T2DM and AD. These findings suggest that *B. vulgaris* leaf extract may offer therapeutic benefits for the management of these diseases.

Author Contributions

Gideon Ampoma Gyebi: data curation, formal analysis, investigation, software, visualization, writing – original draft, writing – review and editing. **Damilare Emmanuel Rotimi:** data curation, methodology, writing – original draft, writing–review and editing. **Moyosoreoluwa Oduba:** data curation, formal analysis, investigation, methodology, writing – original draft. **Ifeoma Nnonyelu:** data curation, formal analysis, investigation, methodology, writing – original draft. **Matthew Iyobhebhe:** methodology, visualization, writing – review and editing. **Musiliyu Ayofe Salawu:** methodology, visualization, writing – original draft. **Adebola Busola Ojo:** data curation, methodology, project administration, writing – review and editing. **Odunayo Anthonia Taiwo:** Validation, visualization, writing – review and editing. **Adesoji Alani Olanrewaju:** software, validation, writing – review and editing. **Abel Kolawole Oyebamiji:** software, validation, visualization, writing – review and editing. **Mubarak Alruwaili:** funding acquisition, project administration, validation, visualization, writing – review and editing. **Naif H Ali:** funding acquisition, project administration, validation, visualization, writing – review and editing. **Saud A. Alnaaim:** funding acquisition, project administration, validation, visualization, writing – review and editing. **Bshra A. Alsfouk:** funding acquisition, project administration, validation, visualization, writing – review and editing. **Gaber El-Saber Baitha:** funding acquisition, project administration, validation, visualization, writing – review and editing. **Oluwafemi Adeleke Ojo:** conceptualization, data curation, formal analysis, project administration, supervision, writing – original draft, writing – review and editing.

Acknowledgments

Dr. Oluwafemi Ojo has been co-funded by the European Union's Horizon Europe Framework Programme for Research and Innovation 2021–2027 under the Marie Sklodowska-Curie action grant agreement No. 101126611.

Ethics Statement

The study adhered to the approved protocols of the Bowen University Research Ethics Committee approval number: BUI/BCH/2024/0001 and was reported in accordance with the ARRIVE guidelines.

Consent

Informed consent was obtained from all individuals included in this study.

Conflicts of Interest

The authors declare no conflicts of interest.

Data Availability Statement

The raw data supporting the conclusions of this article will be made available by the authors upon request.

References

Abd El-Aziz, N. M., O. M. E. Awad, M. G. Shehata, and S. A. El-Sohaimy. 2021. "Antioxidant and Anti-Acetylcholinesterase Potential of Artichoke Phenolic Compounds." *Food Bioscience* 41: 101006. https://doi.org/10.1016/j.fbio.2021.101006.

Abeysinghe, A. A., R. D. Deshapriya, and C. Udawatte. 2020. "Alzheimer's disease; A Review of the Pathophysiological Basis and Therapeutic Interventions." *Life Sciences* 256: 117996. https://doi.org/10.1016/j.lfs.2020.117996.

Araujo-León, J. A., Z. Cantillo-Ciau, D. V. Ruiz-Ciau, and T. I. Coral-Martínez. 2019. "HPLC Profile and Simultaneous Quantitative Analysis

of Tingenone and Pristimerin in Four Celastraceae Species Using HPLC-UV-DAD-MS." *Revista Brasileira de Farmacognosia* 29, no. 2: 171–176. https://doi.org/10.1016/j.bjp.2018.12.009.

Athanasaki, A., K. Melanis, I. Tsantzali, et al. 2022. "Type 2 Diabetes Mellitus as a Risk Factor for Alzheimer's Disease: Review and Meta-Analysis." *Biomedicines* 10, no. 4: 778. https://doi.org/10.3390/biomedicines10040778.

Chaurasiya, N. D., F. Leon, I. Muhammad, and B. L. Tekwani. 2022. "Natural Products Inhibitors of Monoamine Oxidases—Potential New Drug Leads for Neuroprotection, Neurological Disorders, and Neuroblastoma." *Molecules* 27, no. 13: 4297. https://doi.org/10.3390/molecules27134297.

Chen, Z. R., J. B. Huang, S. L. Yang, and F. F. Hong. 2022. "Role of Cholinergic Signaling in Alzheimer's Disease." *Molecules* 27, no. 6: 1816. https://doi.org/10.3390/molecules27061816.

Dong, Y.-w, M.-l Liao, X.-l Meng, and G. N. Somero. 2018. "Structural Flexibility and Protein Adaptation to Temperature: Molecular Dynamics Analysis of Malate Dehydrogenases of Marine Mollusks." *Proceedings of the National Academy of Sciences* 115, no. 6: 1274–1279. https://doi.org/10.1073/pnas.1718910115.

Egbuna, C., C. G. Awuchi, G. Kushwaha, et al. 2021. "Bioactive Compounds Effective Against Type 2 Diabetes Mellitus: A Systematic Review." *Current Topics in Medicinal Chemistry* 21, no. 12: 1067–1095. https://doi.org/10.2174/1568026621666210509161059.

Erukainure, O. L., C. I. Chukwuma, M. G. Matsabisa, V. F. Salau, N. A. Koorbanally, and M. S. Islam. 2020. "Buddleja Saligna Willd (Loganiaceae) Inhibits Angiotensin-Converting Enzyme Activity in Oxidative Cardiopathy With Concomitant Modulation of Nucleotide Hydrolyzing Enzymatic Activities and Dysregulated Lipid Metabolic Pathways." *Journal of Ethnopharmacology* 248: 112358. https://doi.org/10.1016/j.jep.2019.112358.

Falade, A. O., K. E. Adewole, A. A. Ishola, et al. 2022. "Computational Studies on the Cholinesterase, Beta-Secretase 1 (BACE1) and Monoamine Oxidase (MAO) Inhibitory Activities of Endophytes-Derived Compounds: Toward Discovery of Novel Neurotherapeutics." *Journal of Biomolecular Structure and Dynamics*: 1–15.

Green, A. L., and T. M. A. Haughton. 1961. "Colorimetric Method for the Estimation of Monoamine Oxidase." *Biochemical Journal* 78: 172–176.

Gyebi, G. A., O. M. Ogunyemi, A. A. Adefolalu, et al. 2022. "African Derived Phytocompounds May Interfere With SARS-CoV-2 RNA Capping Machinery Via Inhibition of 2'-O-ribose Methyltransferase: An in Silico Perspective." *Journal of Molecular Structure* 1262: 133019. https://doi.org/10.1016/j.molstruc.2022.133019.

Gyebi, G. A., O. M. Ogunyemi, I. M. Ibrahim, S. O. Afolabi, and J. O. Adebayo. 2021. "'Dual Targeting of Cytokine Storm and Viral Replication in COVID-19 by Plant-Derived Steroidal Pregnanes: An in Silico Perspective." *Computers in Biology and Medicine* 134: 104406. https://doi.org/10.1016/j.compbiomed.2021.104406.

Hardy, J., B. de Strooper, and V. Escott-Price. 2022. "Diabetes and Alzheimer's Disease: Shared Genetic Susceptibility?" *Lancet Neurology* 21, no. 11: 962–964. https://doi.org/10.1016/s1474-4422(22)00395-7.

Hernández-Contreras, K. A., J. A. Martínez-Díaz, M. E. Hernández-Aguilar, D. Herrera-Covarrubias, F. Rojas-Durán, and G. E. Aranda-Abreu. 2023. "Depressive Neuropsychiatric Symptoms and Mild Cognitive Impairment as Part of the Diabetes Mellitus/Alzheimer's Disease Link." *Revista Colombiana de Psiquiatria* 52: S146–S158. https://doi.org/10.1016/j.rcp.2021.10.007.

Iwuozor, K. O., and C. S. Afiomah. 2020. "Nutritional and Phytochemical Properties of *Beta vulgaris Linnaeus*(Chenopodiaceae)–A Review." *Nigerian Journal of Pharmaceutical and Applied Science Research* 9, no. 4: 38–44.

Javaid, N., M. A. Shah, A. Rasul, et al. 2021. "Neuroprotective Effects of Ellagic Acid in Alzheimer's Disease: Focus on Underlying Molecular Mechanisms of Therapeutic Potential." *Current Pharmaceutical Design* 27, no. 34: 3591–3601. https://doi.org/10.2174/1873428mtexnndygx.

Karimi I., N. Yousofvand and B. A. Hussein. 2021. "In Vitro Cholinesterase Inhibitory Action of *Cannabis sativa* L. Cannabaceae and in Silico Study of Its Selected Phytocompounds." *In Silico Pharmacology* 9: 1–15. https://doi.org/10.1007/s40203-021-00075-0.

Khan, H., S. Amin, M. A. Kamal, and S. Patel. 2018. "Flavonoids as Acetylcholinesterase Inhibitors: Current Therapeutic Standing and Future Prospects." *Biomedicine & Pharmacotherapy* 101: 860–870. https://doi.org/10.1016/j.biopha.2018.03.007.

Kollman, P. A., I. Massova, C. Reyes, et al. 2000. "Calculating Structures and Free Energies of Complex Molecules: Combining Molecular Mechanics and Continuum Models." *Accounts of Chemical Research* 33, no. 12: 889–897. https://doi.org/10.1021/ar000033j.

Lee, J., X. Cheng, J. M. Swails, et al. 2016. "'CHARMM-GUI Input Generator for NAMD, GROMACS, AMBER, Openmm, and CHARMM/OpenMM Simulations Using the CHARMM36 Additive Force Field." *Journal of Chemical Theory and Computation* 12, no. 1: 405–413. https://doi.org/10.1021/acs.jctc.5b00935.

Lee, J., M. Hitzenberger, M. Rieger, N. R. Kern, M. Zacharias, and W. Im. 2020. "CHARMM-GUI Supports the Amber Force Fields." *Journal of Chemical Physics* 153, no. 3: 035103. https://doi.org/10.1063/5.0012280.

Loukili, E. H., B. Bouchal, M. Bouhrim, et al. 2022. "Chemical Composition, Antibacterial, Antifungal and Antidiabetic Activities of Ethanolic Extracts of Opuntia dillenii Fruits Collected From Morocco." *Journal of Food Quality* 2022: 15. https://doi.org/10.1155/2022/9471239.

Lynn, J., M. Park, C. Ogunwale, and G. K. Acquaah-Mensah. 2022. "A Tale of Two Diseases: Exploring Mechanisms Linking Diabetes Mellitus With Alzheimer's Disease." *Journal of Alzheimer's Disease* 85, no. 2: 485–501. https://doi.org/10.3233/jad-210612.

Miller III, B. R., T. D. McGee Jr, J. M. Swails, N. Homeyer, H. Gohlke, and A. E. Roitberg. 2012. "MMPBSA. Py: An Efficient Program for End-State Free Energy Calculations." *Journal of Chemical Theory and Computation* 8, no. 9: 3314–3321. https://doi.org/10.1021/ct300418h.

Moreira, N. C., J. E. Lima, M. F. Marchiori, I. Carvalho, and E. T. Sakamoto-Hojo. 2022. "Neuroprotective Effects of Cholinesterase Inhibitors: Current Scenario in Therapies for Alzheimer's Disease and Future Perspectives." *Journal of Alzheimer's disease reports* 6, no. 1: 177–193. https://doi.org/10.3233/adr-210061.

Morris, G. M., R. Huey, W. Lindstrom, et al. 2009. "AutoDock4 and AutoDockTools4: Automated Docking With Selective Receptor Flexibility." *Journal of Computational Chemistry* 30, no. 16: 2785–2791. https://doi.org/10.1002/jcc.21256.

Munsamy, G., and M. E. Soliman. 2019. "Unveiling a New Era in Malaria Therapeutics: A Tailored Molecular Approach Toward the Design of Plasmepsin IX Inhibitors." *Protein Journal* 38, no. 6: 616–627. https://doi.org/10.1007/s10930-019-09871-2.

O'Boyle, N. 2011. "Banck M. James CA Morley C. Vandermeersch T. Hutchison GR Open Babel: An Open Chemical Toolbox." *Journal of Cheminformatics* 3, no. 1: 33.

Ogunyemi, O. M., G. A. Gyebi, I. M. Ibrahim, et al. 2023. "Identification of Promising Multitargeting Inhibitors of Obesity From Vernonia Amygdalina Through Computational Analysis." *Molecular Diversity* 27, no. 1: 1–25. https://doi.org/10.1007/s11030-022-10397-6.

Ogunyemi, O. M., G. A. Gyebi, I. M. Ibrahim, et al. 2021. "Dietary Stigmastane-type Saponins as Promising Dual-Target Directed Inhibitors of SARS-CoV-2 Proteases: A Structure-based Screening." *RSC Advances* 11, no. 53: 33380–33398. https://doi.org/10.1039/d1ra05976a.

Ojo, A. B., G. Gyebi, O. Alabi, M. Iyobhebhe, C. O. Nwonuma, and O. A. Ojo. 2022. "*Syzygium aromaticum* (L.) Merr. & L.M.Perry Mitigates Iron-

Mediated Oxidative Brain Injury by Modulation of Redox Imbalance, Cholinergic and Purinergic Dysfunctions, and Glucose Metabolizing Enzymes Activities." *Journal of Molecular Structure* 1268C, no. 2022: 133675. https://doi.org/10.1016/j.molstruc.2022.133675.

Ojo, O. A., A. O. Agboola, O. B. Ogunro, et al. 2023. "Beet Leaf (*Beta Vulgaris L.*) Extract Attenuates Iron-Induced Testicular Toxicity: Experimental and Computational Approach." *Heliyon* 9, no. 7: e17700. https://doi.org/10.1016/j.heliyon.2023.e17700.

Ojo, O. A., G. A. Gyebi, E. H. Ezenabor, et al. 2024. "Exploring Beetroot (*Beta Vulgaris* L.) for Diabetes Mellitus and Alzheimer's Disease Dual Therapy: In Vitro and Computational Studies." *RSC Advances* 14, no. 27: 19362–19380. https://doi.org/10.1039/d4ra03638g.

Ojo, O. A., A. D. Ogunlakin, G. A. Gyebi, et al. 2023. "GC–MS Chemical Profiling, Antioxidant, Anti-Diabetic, and Anti-Inflammatory Activities of Ethyl Acetate Fraction of Spilanthes filicaulis (Schumach. and Thonn.) C.D. Adams Leaves: Experimental and Computational Studies." *Frontiers in Pharmacology* 14: 1235810. https://doi.org/10.3389/fphar.2023.1235810.

Ojo, O. A., A. D. Ogunlakin, G. A. Gyebi, et al. 2023. "Profiling the Antidiabetic Potential of GC–MS Compounds Identified From the Methanolic Extract of *Spilanthes Filicaulis*: Experimental and Computational Insight." *Journal of Biomolecular Structure and Dynamics* 43, no. 3: 1392–1413. https://doi.org/10.1080/07391102.2023.2291828.

Ojo, O. A., A. B. Ojo, C. Okolie, et al. 2021. "Deciphering the Interactions of Bioactive Compounds in Selected Traditional Medicinal Plants Against Alzheimer's Diseases Via Pharmacophore Modeling, Autoqsar, and Molecular Docking Approaches." *Molecules* 26, no. 7: 1996. https://doi.org/10.3390/molecules26071996.

Padeiro, M., P. Santana, and M. Grant. 2023. "Global Aging and Health Determinants in a Changing World." In *Aging* 1, 3–30. Academic Press. https://doi.org/10.1016/b978-0-12-823761-8.00021-5.

Perry, N. S., P. J. Houghton, A. Theobald, P. Jenner, and E. K. Perry. 2000. "In-Vitro Inhibition of Human Erythrocyte Acetylcholinesterase by Salvia Lavandula Efolia Essential Oil and Constituent Terpenes." *Journal Pharmaceutical* 52, no. 7: 895–902. https://doi.org/10.1211/0022357001774598.

Reed, J., S. Bain, and V. Kanamarlapudi. 2021. "A Review of Current Trends With Type 2 Diabetes Epidemiology, Etiology, Pathogenesis, Treatments and Future Perspectives." *Diabetes, Metabolic Syndrome and Obesity* 10: 3567–3602.

Richter, E., T. Geetha, D. Burnett, T. L. Broderick, and J. R. Babu. 2023. "The Effects of Momordica Charantia on Type 2 Diabetes Mellitus and Alzheimer's Disease." *International Journal of Molecular Sciences* 24, no. 5: 4643. https://doi.org/10.3390/ijms24054643.

Sánchez-Martínez, J. D., M. Bueno, G. Alvarez-Rivera, J. Tudela, E. Ibañez, and A. Cifuentes. 2021. "In Vitro Neuroprotective Potential of Terpenes From Industrial Orange Juice Byproducts." *Food & Function* 12, no. 1: 302–314. https://doi.org/10.1039/d0fo02809f.

Santana Azevedo, L., F. Pretto Moraes, X. M. Morrone, et al. 2012. "Recent Progress of Molecular Docking Simulations Applied to Development of Drugs." *Current Bioinformatics* 7, no. 4: 352–365. https://doi.org/10.2174/157489312803901063.

Shai, L., P. Masoko, M. Mokgotho, et al. 2010. "Yeast Alpha Glucosidase Inhibitory and Antioxidant Activities of Six Medicinal Plants Collected in Phalaborwa, South." *South African Journal of Botany* 76, no. 3: 465–470. https://doi.org/10.1016/j.sajb.2010.03.002.

Silva, S. G., R. A. da Costa, M. S. de Oliveira, et al. 2019. "Chemical Profile of Lippia Thymoides, Evaluation of the Acetylcholinesterase Inhibitory Activity of Its Essential Oil, and Molecular Docking and Molecular Dynamics Simulations." *PLoS One* 14, no. 3: e0213393. https://doi.org/10.1371/journal.pone.0213393.

Sun, Y., C. Ma, H. Sun, et al. 2020. "Metabolism: A Novel Shared Link Between Diabetes Mellitus and Alzheimer's Disease." *Journal of Diabetes Research* 2020: 1–12. https://doi.org/10.1155/2020/4981814.

Tinajero, M. G., and V. S. Malik. 2021. "An Update on the Epidemiology of Type 2 Diabetes: A Global Perspective." *Endocrinology and Metabolism Clinics* 50, no. 3: 337–355. https://doi.org/10.1016/j.ecl.2021.05.013.

Trott, O., and A. J. Olson. 2010. "Autodock Vina: Improving the Speed and Accuracy of Docking With a New Scoring Function, Efficient Optimization, and Multithreading." *Journal of Computational Chemistry* 31, no. 2: 455–461. https://doi.org/10.1002/jcc.21334.

Valdés-Tresanco, M. S., M. E. Valdés-Tresanco, P. A. Valiente, and E. Moreno. 2021. "gmx_MMPBSA: A New Tool to Perform End-State Free Energy Calculations With GROMACS." *Journal of Chemical Theory and Computation* 17, no. 10: 6281–6291. https://doi.org/10.1021/acs.jctc.1c00645.

Wang, Y. Z., L. Meng, Q. S. Zhuang, and L. Shen. 2021. "Screening Traditional Chinese Medicine Combination for Cotreatment of Alzheimer's Disease and Type 2 Diabetes Mellitus by Network Pharmacology." *Journal of Alzheimer's Disease* 80, no. 2: 787–797. https://doi.org/10.3233/jad-201336.

Supporting Information

Additional supporting information can be found online in the Supporting Information section.